New Journal of Physics
The open access journal at the forefront of physics

Deutsche Physikalische Gesellschaft DPG IOP Institute of Physics

OPEN ACCESS

Ultra-high energy cosmic ray production in the polar cap regions of black hole magnetospheres

To cite this article: A Yu Neronov *et al* 2009 *New J. Phys.* **11** 065015

View the article online for updates and enhancements.

You may also like

- Constraining Low-luminosity Gamma-Ray Bursts as Ultra-high-energy Cosmic Ray Sources Using GRB 060218 as a Proxy
Filip Samuelsson, Damien Bégué, Felix Ryde et al.

- THE ROLE OF STRUCTURED MAGNETIC FIELDS ON CONSTRAINING PROPERTIES OF TRANSIENT SOURCES OF ULTRA-HIGH-ENERGY COSMIC RAYS
Hajime Takami and Kohta Murase

- DO ULTRAHIGH ENERGY COSMIC RAYS COME FROM ACTIVE GALACTIC NUCLEI AND *FERMI* -RAY SOURCES?
Yun-Ying Jiang, L. G. Hou, J. L. Han et al.

This content was downloaded from IP address 74.208.59.24 on 23/08/2026 at 16:33

New Journal of Physics
The open-access journal for physics

Ultra-high energy cosmic ray production in the polar cap regions of black hole magnetospheres

A Yu Neronov[1,2,5], **D V Semikoz**[3,4] **and I I Tkachev**[4]
[1] ISDC, Ch. d'Ecogia 16, Verosoix 1290, Switzerland
[2] Geneva Observatory, Ch. des Maillettes, Versoix 1290, Switzerland
[3] APC, 10 rue Alice Domon et Leonie Duquet, F-75205 Paris Cedex 13, France
[4] Institute for Nuclear Researches of the Russian Academy of Sciences, 60th October Anniversary Prosp 7a, 117312 Moscow, Russia
E-mail: Andrii.Neronov@unige.ch

New Journal of Physics **11** (2009) 065015 (28pp)
Received 2 October 2008
Published 30 June 2009
Online at http://www.njp.org/
doi:10.1088/1367-2630/11/6/065015

Abstract. We develop a model of ultra-high energy cosmic ray (UHECR) production via acceleration in a rotation-induced electric field in vacuum gaps in the magnetospheres of supermassive black holes (BHs). We show that if the poloidal magnetic field near the BH horizon is misaligned with the BH rotation axis, charged particles, which initially spiral into the BH along the equatorial plane, penetrate into the regions above the BH 'polar caps' and are ejected with high energies to infinity. We show that in such a model acceleration of protons near a BH of typical mass 3×10^8 solar masses is possible only if the magnetic field is almost aligned with the BH rotation axis. We find that the power of anisotropic electromagnetic emission from an UHECR source near a supermassive BH should be at least 10–100 times larger than the UHECR power of the source. This implies that if the number of UHECR sources within the 100 Mpc sphere is $\sim$100, the power of electromagnetic emission that accompanies proton acceleration in each source, 10^{42-43} erg s^{-1}, is comparable to the typical luminosities of active galactic nuclei (AGN) in the local Universe. We also explore the acceleration of heavy nuclei, for which the constraints on the electromagnetic luminosity and on the alignment of the magnetic field in the gap are relaxed.

[5] Author to whom any correspondence should be addressed.

 © IOP Publishing Ltd and Deutsche Physikalische Gesellschaft

Contents

1. Introduction

The existence of the Greisen–Zatsepin–Kuzmin (GZK) cutoff [1, 2] in the spectrum of ultra-high energy cosmic rays (UHECR), found by the High Resolution Fly's Eye (HiRes) experiment [3] and confirmed recently by the Pierre Auger Observatory (PAO) [4], points to the astrophysical origin of the primary cosmic ray (CR) particles. In this case, most of the CRs with energies above the cut-off energy $E \simeq 10^{20}$ eV should come from nearby sources located at a distance $D < 100$ Mpc. At the energies $\sim 10^{20}$ eV the trajectories of the CR protons are not significantly deflected by magnetic fields, so that the UHECR should point directly to their sources. However, the statistics of UHECR events was not enough, up to recently, to identify the population of astronomical sources responsible for the UHECR production.

The first attempt to identify the CR sources via a direct back tracing of UHECR events back to their sources was reported by the PAO collaboration [5, 6], that found evidence for the correlation between the arrival directions of the UHECR and directions toward the nearby active galactic nuclei (AGN). The correlation signal was found at rather small angles with a large number of different AGN contributing to it, and therefore it was interpreted as being caused by proton primaries. However, the data presented in [5, 6] are not really consistent with such an AGN hypothesis [7] and correlations with AGN are absent in the more recent HiRes data [11]. Moreover, a different interpretation of the Auger correlation signal is possible [7]–[10], with just a few sources (or even a single source such as Cen A) contributing in the relevant part of the local Universe and with heavier nuclei making up a substantial fraction of the flux. There is yet another difficulty with the AGN interpretation of the Auger signal. Local AGN are weak, hosting black holes (BHs) of small mass in their hearts, and without strong jets. Acceleration of protons to the highest energies in such AGN is not expected, for a discussion of this issue with respect to the Auger signal see [12]–[14].

It is clear that an increase of the event statistics will lead to further improvement of our knowledge of the astronomical sources of UHECR. It is, however, also clear that even with the increase of the statistics (this requires accumulation of the signal over many years) the sensitivity of the UHECR experiments would not be enough to pinpoint the individual UHECR sources. Even if the class of objects that produce the observed UHECR flux were determined (say, a certain type of AGN), only very limited information about the location of the particle acceleration sites and physical conditions in these sources would be extractable from the UHECR data alone.

Assuming that at least some of AGN are potential sources [15], different 'candidate' UHECR acceleration sites can be studied in detail in relation to the Auger signal, such as the giant radio lobes of radio galaxies [16, 17], the large-scale jets [18] or the AGN central engine. The only way to study the acceleration mechanisms in the individual UHECR sources is to single out the signal related to the UHECR production and propagation in the broad band electromagnetic spectrum or to detect the high-energy neutrino emission from the source.

Recent observations of fast variability of the very-high-energy (VHE) γ-ray emission from a nearby radio-galaxy M87 [19] and from several blazars, Mkn 501 [20] and PKS 2155-304 [21], strengthen the conjecture that the central engines of AGN, the supermassive BHs, could operate as powerful particle accelerators [22]–[24]. The observed variability timescales, which are of the order of, or shorter than the light-crossing times of the BH horizons, put tight constraints on the possible locations of particle accelerators in these objects.

The compactness of the accelerators operating in the vicinity of the supermassive BHs (the characteristic size scale is set up by the Schwarzschild radius, $R_{\rm Schw} = 2GM \simeq 3 \times 10^{13}[M/10^8 M_\odot]$ cm, where M is the BH mass and G is Newton's constant) makes particle acceleration in these objects difficult, because of the inevitably strong energy losses related to the synchrotron/curvature radiation of the accelerated particles (see e.g. [25]–[27]). The fact that, in spite of the strong energy loss rate, these accelerators produce electrons with energies of at least 10–100 TeV (the spectrum of the radio galaxy M87 extends at least up to 20 TeV without a signature of a cutoff), implies that the mechanism of acceleration operating in these objects is highly efficient [22]. An obvious candidate for such a highly efficient (i.e. fast) acceleration mechanism is acceleration of charged particles in a strong large-scale electric field, which can be induced in the BH magnetosphere e.g. via the rotational drag of the magnetic field by the BH, or in the regions of magnetic field reconnection in the accretion disc.

Large-scale ordered electric fields, induced by rotation of the compact object, are known to be responsible for particle acceleration and high-energy radiation in pulsars (see e.g. [28]). In the case of pulsars, it is known that particles are accelerated in the so-called 'vacuum gaps' in the magnetosphere, in which the rotation-induced electric field is not neutralized by redistribution of charges. A similar mechanism of generation of large electric fields can be realized in the vicinity of a rotating BH [29, 30]. Moreover, it has been argued that vacuum gaps should also form in the vicinity of a rotating BH [31]–[34], which means that a mechanism of particle acceleration similar to the one operating in pulsars should work also in BH-powered sources. The observational consequences of acceleration in the vacuum gaps of BH magnetospheres were studied as a possible mechanism of powering the AGN jet [31, 35, 36] and neutrino emission [37] from AGN.

The possibility of UHECR generation near the supermassive BH in the nuclei of normal galaxies (the so-called 'dead quasars') was studied in [25, 27, 38]. As mentioned above, in this particular case, the compactness of the source makes the acceleration to UHECR energies ($>10^{20}$ eV) only marginally possible. A numerical study of the limit on the maximal energies attainable by the accelerated protons reported in [27] has revealed that, in general, acceleration to energies above 10^{20} eV is possible only in the vicinity of the most massive BHs (with masses of the order of $10^{10} M_{\odot}$), which are relatively rare. Besides, such acceleration is accompanied by strong electromagnetic emission, with a luminosity about 2–3 orders of magnitude higher than the UHECR luminosity of the source. This implies that the electromagnetic luminosity of each of the UHECR sources should be at the level of $10^{45-46}/N_{\rm source}\,{\rm erg\,s^{-1}}$, where $N_{\rm source}$ is the number of the nearby UHECR sources (a typical distance to the source $D \sim 50$ Mpc is assumed). If the number of UHECR sources is not very large, such a luminosity is about the luminosity of the quasars. This, apparently, rules out the model of particle acceleration near the supermassive BHs in nearby normal galaxies (the 'dead quasars' [38]) as a possible mechanism of UHECR production in nearby sources [27].

The results of [27] were obtained for the case of acceleration of protons and under the assumption of a general orientation of the magnetic field (created by matter accreting onto the BH) with respect to the rotation axis of the BH.

The assumption of the absence of alignment between the direction of the magnetic field and the BH rotation axis was justified in the context of the dead quasar model of the environment of a supermassive BH. In contrast, steady AGN activity in the source would result in the production of a stationary accretion disc whose rotation axis is almost aligned with the rotation axis of the BH [39]. Such an alignment would lead to the alignment of the magnetic field with the BH rotation axis. In this paper, we investigate (both analytically and numerically) the consequence of alignment of the magnetic field with the BH rotation axis for particle acceleration. We show that if the magnetic field is aligned to within several degrees, production of ultra-high energy protons becomes possible even for BHs of moderate mass ($M \sim 10^8 M_{\odot}$), provided that the magnetic field is very strong ($\sim 10^5$ G). We also show that the constraint on the strength and alignment of the magnetic field is largely relaxed in the case of acceleration of heavy nuclei to ultra-high energies ($\geqslant 10^{20}$ eV).

The assumptions of alignment of the magnetic field with the BH rotation axis and/or of acceleration of heavy nuclei also lead to a decrease of the estimate of the power of electromagnetic radiation that accompanies the acceleration. In these cases, the electromagnetic luminosity of the vacuum gap at least does not exceed the typical luminosities of the AGN in the local Universe.

The plan of the paper is as follows. In section 2, we discuss the possible location, geometry and physical conditions in the vacuum gaps close to the BH horizon. To make the presentation self-contained, we give the exact expressions for the rotation-induced electric field around a BH placed in an external magnetic field inclined with respect to the rotation axis. In section 3, we discuss the motion of a charged particle in external gravitational and electromagnetic fields near the BH. In section 4, we present the results of numerical modelling of such motion and find the dependence of the maximal energies of protons accelerated by the rotation-induced electric field on the main geometrical and physical parameters of the vacuum gap. We find that for reasonable assumptions about the BH mass and the strength of the magnetic field, the acceleration of protons to UHECR energies is possible only in the case when the magnetic field is almost aligned with the rotation axis of the BH (it remains to be seen if such an alignment can be achieved in nature). In section 5 we calculate, analytically and numerically, the electromagnetic luminosity of the gap and find that the alignment of the magnetic field with the rotation axis reduces the γ-ray luminosity of the gap (making the estimate of the electromagnetic power compatible with the estimates of the luminosity of typical AGN in the local Universe). We find that, apart from the boosting of the maximal energies of accelerated particles and reduction of the electromagnetic power, the alignment of the magnetic field with the rotation axis results in reduction of the probability of the onset of pair production inside the gap which would lead to a 'discharge' of the gap and neutralization of the large-scale electric field. In section 6, we explore the acceleration of heavy nuclei in the vacuum gaps and show that, contrary to the case of proton acceleration, the energies of nuclei can reach 10^{20} eV already at moderate magnetic field strength and in the absence of alignment of the magnetic field with the rotation axis. Finally, in section 7 we summarize our results.

2. Vacuum gaps in the BH magnetosphere

2.1. BH magnetosphere

In the models of the most powerful AGN, accretion is assumed to proceed at nearly the maximal possible (Eddington) rate at which the gravitational attraction by the BH starts to be balanced by the pressure of radiation produced by the accretion flow. In this regime the accretion flow forms a geometrically thin, optically thick accretion disc [40], emitting thermal radiation, which, in the case of AGN, is usually identified with the so-called 'big blue bump' in the ultra-violet part of the AGN spectrum. When the accretion rate onto the BH is sufficiently below the Eddington rate, the accretion proceeds in a 'radiatively inefficient' regime, in which most of the released gravitational energy of the accreting matter is converted into internal energy, rather than into radiation. This energy is subsequently advected by the BH or ejected with a matter outflow [41]. In this regime, the large internal energy of matter does not allow formation of a gemetrically thin accretion disc. Instead, the accreting matter forms a hot, optically thin gaseous torus around the BH [42].

In both accretion regimes, the structure of the accretion flow close to the BH is significantly affected by the presence of strong magnetic field. The details of the structure of the magnetic field play, in fact, a determining role in the dynamics of matter in the regions in which the magnetic field energy density $U_B = B^2/8\pi$ dominates over the kinetic energy density of the accreting matter $U_k = \rho v^2/e$, i.e. in the regions where the magnetization parameter $\sigma = U_B/U_k > 1$. Even though the density of matter in the magnetized regions is very low, it is usually supposed to be sufficient to neutralize the large-scale electric field component parallel to the magnetic field lines, which otherwise would be induced by the rotation of the magnetic field and of the space–time around the BH (see below). The characteristic charge density needed to neutralize the parallel component of the electric field in the magnetosphere of a BH of mass M rotating with an angular velocity $\vec{\Omega}$ placed in an external magnetic field $\vec{B}$ is the so-called 'Goldreich-Julian' (GJ) density [43]

$$n_q \sim \frac{\vec{\Omega} \cdot \vec{B}_{\text{ord}}}{e} \sim \frac{a B_{\text{ord}}}{e(GM)^2}, \tag{1}$$

where G is the gravitational constant, e is the charge of an electron and a is the BH angular momentum per unit mass (we use the natural units $c = \hbar = 1$ throughout the paper). If the density of the plasma in the large magnetization regions is above n_q, the plasma and magnetic fields in the high-magnetization regions form the 'force-free' magnetosphere (in which the electric field is everywhere orthogonal to the magnetic field).

Charged particles can be supplied to the force-free magnetosphere in several ways. First, if the accretion flow generates a poloidal magnetic field penetrating through the accretion disc, particles bound to the magnetic field could be accelerated by a centrifugal force and escape along the poloidal magnetic field lines to the high-magnetization regions and further into a directed outflow [44] (this mechanism is often suggested as the mechanism of launching of collimated jets from BHs). Injection of plasma via such mechanism is possible only along the magnetic field lines at which the centrifugal force dominates over the gravitational force. This condition is not satisfied in the regions close to the BH horizon and/or close to the BH rotation axis. This can lead to the deficiency of supply of charged particles and formation of 'vacuum gaps' in the force-free magnetosphere.

Once the 'force-free' conditions in the vacuum gap in the BH magnetosphere are broken, the presence of a nonzero component of electric field parallel to the magnetic field lines starts to provide a further obstacle for the charge supply in the magnetosphere, leading to a growth of the vacuum gap size. The process of the growth of the vacuum gap can terminate only if the large enough electric field in the gap leads to its 'discharge' similar to the discharge in a capacitor.

The discharge of the gap can provide an additional mechanism of supply of charged particles into the magnetosphere. This mechanism is similar to the one operating in pulsar magnetospheres: particles accelerated in the vacuum gaps can generate e^+e^- pairs via pair production in interactions with the magnetic or radiation fields. Such a mechanism of charge supply is implied e.g. in the Blandford–Znajek scenario [33]. The efficiency of this mechanism of charge supply strongly depends on the strength and inclination of the magnetic field (see section 5.3 below). The efficiency of the charge supply via pair production by γ-rays on the soft infrared background depends on the compactness of the infrared source ($\propto L_{\rm IR}/R$) [22].

Strictly speaking, the geometry and the structure of the electromagnetic field in the vacuum gap in the magnetosphere can be derived only from numerical modelling of the process of formation of the gap. Such a numerical modelling is a complicated task, because the existing numerical codes for modelling of the BH magnetospheres are based on the explicit assumption of the force-free conditions, which simplify the numerical calculations [45]. In fact, the numerical codes have an upper limit on plasma magnetization above which they fail. Because of this difficulty, the existing numerical codes always include an artificial injection of free charges in the points where the vacuum gaps should normally form [45].

At the same time, some of the qualitative features of the particle acceleration in the vacuum gaps could be established via analytical/numerical calculations done in the approximation opposite to the approximation of the force-free magnetosphere, i.e. neglecting the possible nonzero particle density in the vacuum gap. In what follows we adopt such an approximation, leaving the self-consistent calculations of the vacuum gap geometry and particle acceleration in the vacuum gap to future work.

2.2. *Rotation-induced electric field*

A rotating BH placed in an external magnetic field generates an electric field of quadrupole topology via a mechanism similar to the mechanism of generation of a quadrupole electric field by a rotating dipole magnetic field in the case of a neutron star. The only difference is that in the case of the BH the rotation of the external magnetic field arises due to a rotational drag of the external magnetic field, rather than due to the rotation of the star.

An exact solution of the Maxwell equations in the background of Kerr space–time of a rotating BH is known for the case of arbitrary inclination angle of an asymptotically homogeneous magnetic field [29, 30]. In this solution, the rotational drag of magnetic field by the BH leads to the generation of a large-scale electric field close to the BH horizon. This solution can be a first approximation for description of the structure of the electromagnetic field in the vacuum gap in the BH magnetosphere. It is clear, however, that the presence of charge-separated plasma around the gap will, in general, lead to modification of the electromagnetic field structure.

A rotating BH is described by two parameters: its mass M and the angular momentum per unit mass $a < M$ (we use the system of units in which the Newton's constant G_{N} and the speed of light c are equal to 1). The geometry of space–time in the vicinity of the horizon is described by the Kerr metric [46]

$$\mathrm{d}s^2 = -\alpha^2 \mathrm{d}t^2 + g_{ik}\left(\mathrm{d}x^i + \beta^i \mathrm{d}t\right)\left(\mathrm{d}x^k + \beta^k \mathrm{d}t\right), \tag{2}$$

$$\alpha = \frac{\rho\sqrt{\Delta}}{\Sigma}, \quad g_{rr} = \frac{\rho^2}{\Delta}, \quad g_{\theta\theta} = \rho^2, \quad g_{\phi\phi} = \frac{\Sigma^2 \sin^2\theta}{\rho^2}, \tag{3}$$

$$\beta_\phi = -\frac{2aMr}{\Sigma^2}, \quad \Delta = r^2 + a^2 - 2Mr, \tag{4}$$

$$\Sigma^2 = (r^2+a^2)^2 - a^2\Delta\sin^2\theta, \quad \rho^2 = r^2 + a^2\cos^2\theta. \tag{5}$$

The horizon is situated at $r_{\mathrm{H}} = M + \sqrt{M^2 - a^2}$.

The solution of the Maxwell equations, which corresponds to the asymptotically homogeneous magnetic field inclined at an angle χ with respect to the BH rotation axis, is given by the electromagnetic tensor [30]

$$\begin{aligned}
F_{tr} &= \frac{aMB_0}{\rho^4\Delta}\big[\cos\chi\,\Delta(r^2 - a^2\cos^2\theta)(1+\cos^2\theta) + \sin\chi\, r\sin\theta\cos\theta\{(r^3 - 2Mr^2 \\
&\qquad + ra^2(1+\sin^2\theta) + 2Ma^2\cos^2\theta)\cos\psi - a(r^2 - 4Mr + a^2(1+\sin^2\theta))\sin\psi\}\big], \\
F_{t\theta} &= \frac{aMB_0}{\rho^4}\left[2\cos\chi\, r\sin\theta\cos\theta(r^2-a^2) + \sin\chi\,(r^2\cos 2\theta + a^2\cos^2\theta)(a\sin\psi - r\cos\psi)\right], \\
F_{t\phi} &= \frac{B_0\sin\chi\, aM}{\rho^2}\sin\theta\cos\theta(a\cos\psi + r\sin\psi), \\
F_{r\theta} &= -B_0\sin\chi\,(a\cos\psi + r\sin\psi) - \frac{B_0\sin\chi\, a}{\Delta}\big[(Mr - a^2\sin^2\theta)\cos\psi \\
&\qquad - a(r\sin^2\theta + M\cos^2\theta)\sin\psi\big], \\
F_{r\phi} &= B_0\cos\chi\, r\sin^2\theta + a\sin^2\theta\, F_{tr} \\
&\qquad - B_0\sin\chi\,\sin\theta\cos\theta\left[\left(r - a^2M/\Delta\right)\cos\psi - a\,(1 + rM/\Delta)\sin\psi\right], \\
F_{\theta\phi} &= B_0\cos\chi\,\Delta\sin\theta\cos\theta + \frac{(r^2+a^2)}{a}F_{t\theta} \\
&\qquad + B_0\sin\chi\left[(r^2\sin^2\theta + Mr\cos 2\theta)\cos\psi - a(r\sin^2\theta + M\cos^2\theta)\sin\psi\right],
\end{aligned} \tag{6}$$

where

$$\psi = \phi + \frac{a}{2\sqrt{M^2 - a^2}} \ln \left[\frac{r - M + \sqrt{M^2 - a^2}}{r - M - \sqrt{M^2 - a^2}} \right]. \tag{7}$$

In order to understand the qualitative features of an electromagnetic field configuration in a curved space–time (like that of a rotating BH) it is convenient to consider the field geometry in a locally Lorentzian reference frame. In the case of Kerr space–time it is convenient to choose the so-called 'locally non-rotating' reference frame (LNRF), spanned by the orthonormal basis vectors [46]:

$$\begin{aligned} e_{\hat{0}} &= \frac{\Sigma}{\rho\sqrt{\Delta}} \frac{\partial}{\partial t} + \frac{2Mar}{\Sigma\rho\sqrt{\Delta}} \frac{\partial}{\partial \phi}, \\ e_{\hat{r}} &= \frac{\sqrt{\Delta}}{\rho} \frac{\partial}{\partial r}, \\ e_{\hat{\theta}} &= \frac{1}{\rho} \frac{\partial}{\partial \theta}, \\ e_{\hat{\phi}} &= \frac{\rho}{\Sigma \sin\theta} \frac{\partial}{\partial \phi}. \end{aligned} \tag{8}$$

In this reference frame the magnetic and electric field vectors are expressed through the components of the tensor of electromagnetic field $F_{\mu\nu}$, given by equation (6), as

$$B^{\hat{r}} = \frac{F_{\theta\phi}}{\Sigma \sin\theta}, \quad B^{\hat{\theta}} = -\frac{\sqrt{\Delta} F_{r\phi}}{\Sigma \sin\theta}, \quad B^{\hat{\phi}} = \frac{\sqrt{\Delta} F_{r\theta}}{\rho^2}, \tag{9}$$

$$E^{\hat{r}} = \frac{\Sigma F_{tr} - ar F_{r\phi}/\Sigma}{\rho^2}, \quad E^{\hat{\theta}} = \frac{\Sigma F_{t\theta} - ar F_{\theta\phi}/\Sigma}{\rho^2\sqrt{\Delta}}, \quad E^{\hat{\phi}} = \frac{F_{t\phi}}{\sqrt{\Delta}\sin\theta}. \tag{10}$$

The expressions for electric and magnetic fields simplify in the case of a magnetic field aligned with the BH rotation axis, $\chi = 0$. The solution of the Maxwell equations for this particular case was initially reported in [29]. Figure 1 shows the geometry of electric and magnetic field lines for $\chi = 0$ in the case of a maximally rotating BH $a = M$. Taking the asymptotic expression for $\vec{E}$, $\vec{B}$ in the limit $r \to \infty$ one can find that far away from the horizon the electromagnetic field is

$$\begin{aligned} &B^{\hat{r}} \to B_0 \cos\theta, \quad B^{\hat{\theta}} \to -B_0 \sin\theta, \\ &E^{\hat{r}} \to -\frac{B_0 a M (3\cos^2\theta - 1)}{r^2}, \quad E^{\hat{\theta}} = O(r^{-4}). \end{aligned} \tag{11}$$

The electric field has a quadrupole geometry, which is clearly visible in figure 1.

In the regions where electric field has a component along the magnetic field, charged particles can be accelerated. Particles of opposite charge sign are accelerated in opposite

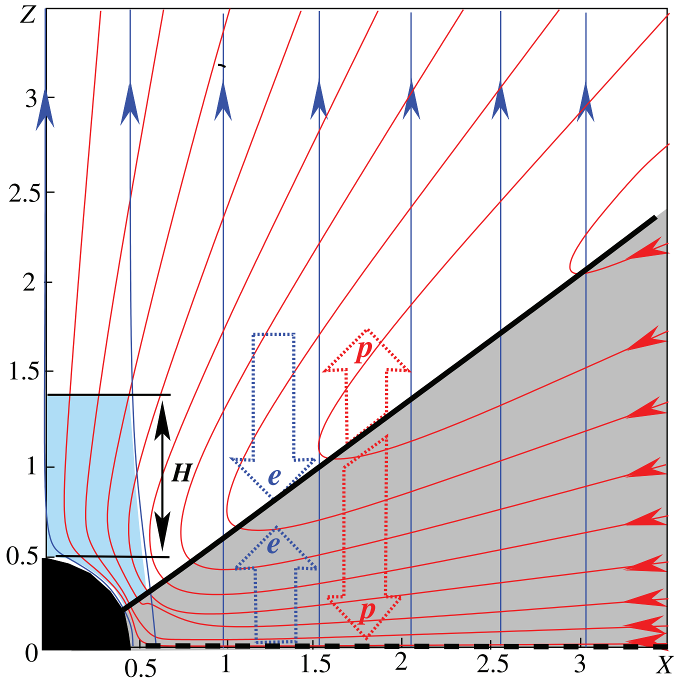

Figure 1. Magnetic (blue solid) and electric (red solid) field lines of the field (6) for $a = M$ and $\chi = 0$. The horizon is situated at $r = 0.5(R_{\mathrm{grav}}) = M$. Wide blue and red arrows show the directions of acceleration of electrons and protons in different regions. Thick solid and dashed lines show the conical and equatorial 'force-free' surfaces. The blue-shaded region shows the location of a vacuum gap into which particles from the equatorial accretion flow can leak if $\chi > 0$.

directions. The acceleration can be avoided only if a particle resides at a surface at which the electric field is orthogonal to the magnetic field (which can be called 'force-free' surfaces), such as the surfaces shown by thick solid and dashed black lines in figure 1. The force-free surfaces separate different acceleration regions (with electric field directed along or opposite to the magnetic field), shown as white ($\vec{E} \cdot \vec{B} > 0$) and grey ($\vec{E} \cdot \vec{B} < 0$) areas in figures 1 and 2.

As one can see from figure 1, the force-free surfaces serve as 'attractors' to the particles of a definite charge sign. In the case of magnetic field aligned with the rotation axis, shown in figure 1, the surface attracting the positively charged particles (the equatorial plane surface) does not intersect with the force-free surface attracting negatively charged particles (shown by the thick solid black curve). However, as soon as the inclination angle of the magnetic field becomes nonzero, the two force-free surfaces 'reconnect' as shown in figure 2. At moderate inclination angles of the magnetic field, the reconnection region is situated close to the equatorial plane, near the BH. The width of the reconnection region grows with increasing inclination angle. In the following sections, we show that charged particles that spiral toward the BH in the equatorial plane, can be accelerated and ejected to infinity when they reach the reconnection region.

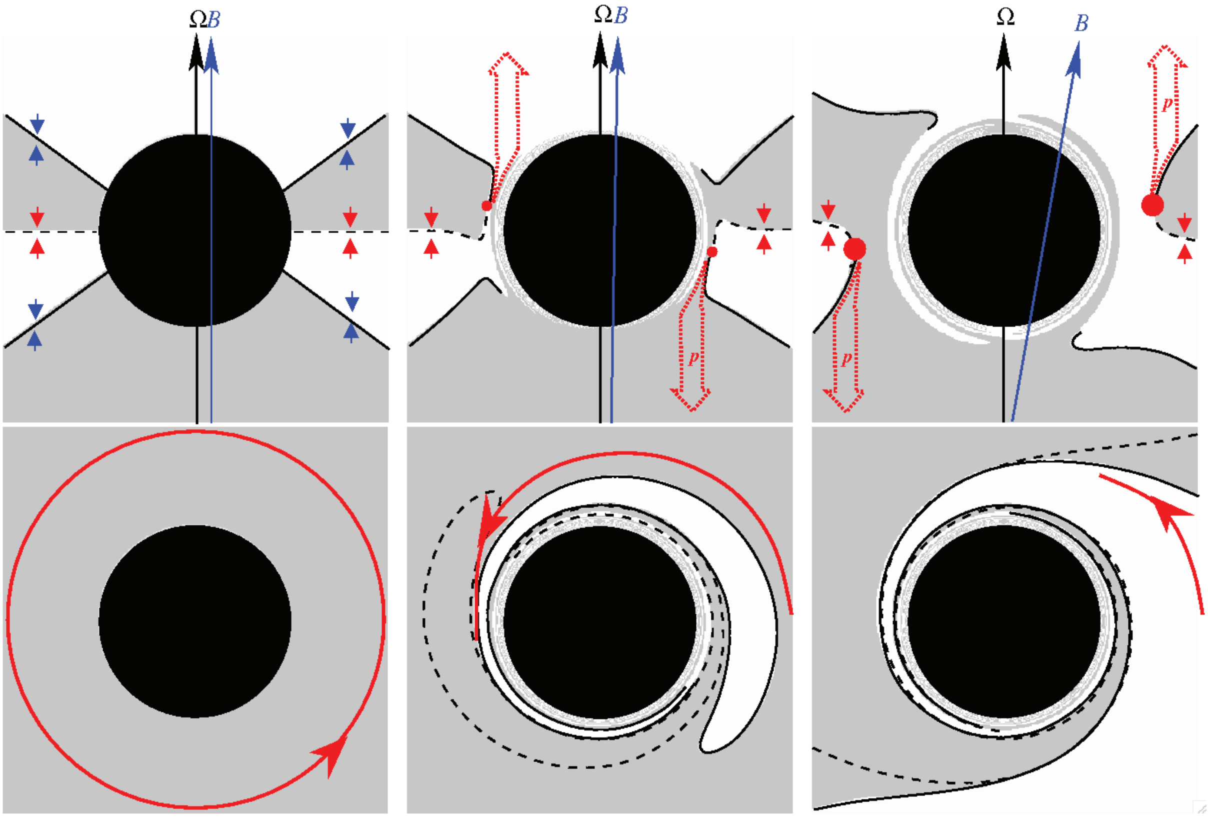

Figure 2. Evolution of the structure of the force-free surfaces with the increasing misalignment of the magnetic field. The equatorial force-free surface, shown by the dashed line, 'reconnects' with the conical force-free surfaces (solid lines) at nonzero inclination angles. The three top panels show the view in the xz plane for the inclination angles $\chi = 0°$, $1°$ and $10°$. The bottom panels show the view in the xy plane (just above the equatorial plane, at $z = 0.01 R_{\mathrm{Schw}}$) for the same inclination angles. The spiral-like reconnection surfaces, which would be visible if the plane $z = -0.01 R_{\mathrm{Schw}}$ were chosen, are shown by the black dashed curves in the middle and right lower panels. White (grey) areas show the regions where the electric field component along the magnetic field lines has positive (negative) sign. Black circles show the horizon of a maximally rotating BH. Depending on the charge sign, particles in-spiralling towards the BH along the equatorial force-free surface are either ejected to infinity (positively charged particles in this figure, whose typical trajectories are shown by red curves) or are trapped in the region between two force-free surfaces.

2.3. Geometry and location of the vacuum gap(s)

In the electromagnetic field configuration around the BH discussed in the previous section, the vacuum gap forms in the region above the BH 'polar cap' if the free charges that can fill the magnetosphere are supplied by the equatorial accretion disc. Extraction of the free charges from the equatorial disc by the rotation-induced electric field will result in the formation of a region filled with electrons, above and below the equatorial disc, up to the conical force-free surface, shown by the black solid thick curve in this figure. However, if the magnetic field is aligned with the rotation axis, the region above the 'polar cap' of the BH will remain free of charge, because there is no way to fill this region via extraction of charges from the equatorial disc. Only if the magnetic field is misaligned with the BH rotation axis can the free charges from the equatorial disc 'leak' into the polar cap passing through the 'reconnection' region of the two force-free surfaces, as shown in figure 2. This will result in charge supply into the region above the 'polar cap', which is shown as a blue-shaded region in figure 1. However, any charged particle that penetrates into this region escapes to infinity along the magnetic field lines, so that the charge distribution in this region should be constantly 'refilled' via the 'leakage' from the equatorial force-free surface.

In principle, the redistribution of the charges supplied from the accretion disc will modify the structure of the electromagnetic field around the BH. The exact location of the vacuum gap(s) in the BH magnetosphere can be found only via numerical modelling of the charge supply and formation of the force-free magnetosphere. Such modelling is difficult already in the case of pulsars, where several 'candidate' sites for the vacuum gap locations are considered, such as the magnetic polar cap regions, 'slot gaps' at the boundaries of regions filled with positively and negatively charged plasmas, 'outer gaps' close to the light cylinder, etc (see e.g. [28]). In the case of the BHs, modelling of the formation of the force-free magnetosphere has an additional difficulty, because the location of the gap can depend on the geometrical pattern of the accretion flow. The gap model considered in the previous section can serve as a useful 'toy model' for the gap geometry.

Within this 'toy model' the gap has a particular geometry shown in figure 1. Charged particles 'leak' from the accretion disc through the region of 'reconnection' of the force-free surfaces (see figure 2). The gap is situated above the BH 'polar cap' and extend along the magnetic field lines up to the height H above the BH horizon. We consider particle acceleration in a gap of such geometry, to establish qualitative features of the vacuum gap acceleration mechanism. Our results can be then generalized, in a straightforward way, to the more complicated (and more realistic) models of vacuum gaps in the BH magnetosphere.

3. Particle acceleration in the vacuum gap

3.1. General properties of particle motion in the vacuum gap

The electromagnetic field in the vacuum gap consists of electric and magnetic fields that are, in general, inclined at a nonzero angle with respect to each other. General properties of particle motion in such an electromagnetic field and in the curved space–time around the BH can be readily understood.

Qualitatively, a particle moving in a magnetic field spirals around the magnetic field lines with a gyroradius

$$R_{\rm gyro} = \frac{E}{qB_0} \approx 10^2 \left[\frac{10^4\,{\rm G}}{B_0}\right]\left[\frac{E}{1\,{\rm GeV}}\right]{\rm cm}, \qquad (12)$$

where E is the energy of the particle and q is its charge. For a particle with an energy $E \ll 10^{20}\,$eV the gyroradius is normally essentially less than the scale of variation of the electromagnetic field which is of the order of $R_{\rm Schw} = 3\times 10^{13}\,[M/10^8 M_\odot]\,$cm. This gyroradius distance scale is also much smaller than the scale at which particle trajectory is significantly affected by the gravitational field of the BH (which is also about R_{Schw}). Therefore, one could separate the distance scales at which electromagnetic and gravitational forces are important. At small scales ($\ll R_{\mathrm{Schw}}$), one can locally approximate particle trajectories as motion in the crossed magnetic and electric fields, forming the field configuration described in section 2.2.

The motion of a charged particle in such an electromagnetic field is composed of the spiraling along the magnetic field lines and the orthogonal drift with velocity

$$v_{\mathrm{drift}} = \frac{\vec{E} \times \vec{B}}{|\vec{B}|^2}. \tag{13}$$

Since in the case of interest $|E| \sim |B|$, $v_{\mathrm{drift}} \sim c$ and, in general, particle trajectories significantly deviate from a simple spiralling along the magnetic field lines. For example, the drift velocity of particles moving in the equatorial plane near the BH placed in the magnetic field, aligned with the BH rotation axis, is directed along a circle around the BH, so that the particles drift along the circular trajectories (red circle in the left bottom panel of figure 2). If the magnetic field is slightly mis-aligned with the rotation axis, the particles spiral into (or away from) the BH, rather than move along the circular orbits (red curves in the middle and right bottom panels of figure 2). The particles that spiral in reach the region of 'reconnection' of the force-free surfaces (red dots in figure 2) and are finally either ejected into the 'polar cap' region or fall under the BH horizon.

Apart from spiralling along the magnetic field lines and drift across the field lines, particles can be accelerated by the electric field. Only the presence of the electric field component along the magnetic field line can lead to the increase or decrease of particle energy. Obviously, positively charged particles are accelerated in the direction opposite to the direction of acceleration of negatively charged particles. Depending on the location of the point of injection of a low-energy particle (e.g. proton or electron) into the reconnection region, the particle can be accelerated in such a way that it either escapes 'to infinity' along the direction of magnetic field lines, or it is trapped in a finite region between the neighbouring force-free surfaces close to the horizon.

3.2. Maximal energies of accelerated particles

Neglecting the energy losses, the maximal energies attainable for nuclei of the charge Ze are determined by the available potential difference in the gap, $U \sim ER \sim aBR$,

$$E_{\mathrm{max}} = ZeBR \simeq 10^{20} Z \left[\frac{B}{10^4\,\mathrm{G}}\right] \left[\frac{M}{10^8 M_\odot}\right] \mathrm{eV}. \tag{14}$$

In a realistic situation, the energy losses of the accelerated particles (e.g. on the electromagnetic radiation associated with the accelerated motion of the particle) limit the maximal energies to values below the estimate of equation (14).

In particular, the accelerated nuclei inevitably suffer from the curvature radiation loss

$$\frac{\mathrm{d}E}{\mathrm{d}t} = -\frac{2Z^2e^2E^4}{3A^4m_{\mathrm{p}}^4R^2}, \tag{15}$$

where m_{p} is the proton mass and A is the atomic number. In the electromagnetic field configuration (6), describing a magnetic field almost aligned with the BH rotation axis, the curvature radius of magnetic field lines in the gap scales roughly as $R \simeq R_{\rm Schw}/\chi$. Equating the acceleration rate $\mathrm{d}E/\mathrm{d}t \sim ZeB$ to minus the energy loss rate (15), one arrives at the following estimate of the maximum energy:

$$
\begin{aligned}
E_{\rm cur} &= \left[\frac{3A^4m^4R^2B}{2Ze\chi^2}\right]^{1/4} \\
&\simeq 8\times 10^{19} A Z^{-1/4}\left[\frac{M}{10^8 M_\odot}\right]^{1/2}\left[\frac{B}{10^4\,\mathrm{G}}\right]^{1/4}\left[\frac{\chi}{1^\circ}\right]^{-1/2}\ \mathrm{eV}.
\end{aligned} \tag{16}
$$

The range of applicability of equation (16) is given by the condition $B > B_{\rm crit}$, where $B_{\rm crit}$ is found from the requirement $E_{\rm cur} = E_{\rm max}$:

$$
\begin{aligned}
B_{\rm crit} &= \left[\frac{3A^4m_{\rm p}^4}{2Z^5e^5R^2\chi^2}\right]^{1/3} \\
&\simeq 10^4 A^{4/3} Z^{-5/3}\left[\frac{M}{10^8 M_\odot}\right]^{-2/3}\left[\frac{\chi}{1^\circ}\right]^{-2/3}\ \mathrm{G}.
\end{aligned} \tag{17}
$$

This critical field corresponds to particle energy

$$
E_{\rm crit} \approx 10^{20} A^{4/3} Z^{-2/3}\left[\frac{M}{10^8 M_\odot}\right]^{1/3}\left[\frac{\chi}{1^\circ}\right]^{-2/3}\ \mathrm{eV}. \tag{18}
$$

The above estimates show that it is possible to accelerate protons or heavier nuclei to energies about 10^{20} eV in the central engines of typical AGNs, with BH masses around 10^8 solar masses. The necessary condition for such acceleration is that the curvature radius of particle trajectories should be much larger (by a factor $1/\chi$) than $R_{\rm Schw}$. This can be achieved in the 'polar cap' regions if the magnetic field is moderately misaligned with the BH rotation axis.

4. Numerical modelling of particle acceleration in the gap

In order to study the dependence of the maximal energies of the accelerated particles on the parameters of the model (in particular, on the BH mass M, magnetic field B and inclination angle χ of the magnetic field with respect to the BH rotation axis), we have developed a numerical code that traces the particle trajectories through the electromagnetic field configuration described in section 2 taking account of the energy loss on the emission of synchrotron/curvature radiation. To study the electromagnetic luminosity of the vacuum gap, we also model the propagation of photons emitted by the accelerated particles through the BH space–time.

4.1. Numerical code

We have developed a numerical code to model charged particle motion in the curved space–time and in the electromagnetic field configuration described section 2.2. For this we have first written the equations of motion of a charged particle in the LNRF (see equation (8)) [47]

$$
\frac{\mathrm{d}\vec{p}}{\mathrm{d}\hat{t}} = e(\vec{E} + \vec{v}\times\vec{B}) + m\gamma\vec{g} + \hat{H}\vec{p} + \vec{f}_{\rm rad}, \tag{19}
$$

where $\vec{p}$ is the particle momentum

$$p^{\hat{a}} = m\gamma v^{\hat{a}}, \tag{20}$$

(hats denote the vector components in the LNRF) $\vec{g}$ is the gravitational acceleration and $\hat{H}$ is the tensor of gravi-magnetic force. The force $\vec{f}_{\mathrm{rad}}$ is the radiation reaction force and $v^{\hat{a}}$ is the 3-velocity of the particle in the LNRF. Next, taking into account the fact that the motion of a charged particle involves many distance scales, from the gyroradius R_{gyro} (12) up to R_{Schw}, we have found that a step of the numerical integration is determined by the smallest scale involved (R_{gyro} most of the time). At this length scale the motion of the particle can be modelled in the LNRF by a numerical integration of equation (20). Using the book [48], we have written a code which integrates the above equations numerically. The elementary step of the numerical integration increases or decreases along the particle trajectory, together with the increase or decrease of the energy of the particle (see equation (12)).

The radiation reaction force $\vec{f}_{\mathrm{rad}}$ for the ultra-relativistic particles moving in an external electromagnetic field is (see e.g. [49])

$$\vec{f}_{\mathrm{rad}} = \frac{2e^4\gamma^2}{3m^2}\left((\vec{E}+\vec{v}\times\vec{B})^2 - (\vec{v}\cdot(\vec{E}+\vec{v}\times\vec{B}))^2\right)\frac{\vec{v}}{|v|}. \tag{21}$$

Note that if particles move at large angle with respect to the magnetic field lines, this expression will describe mostly synchrotron energy loss. However, in the case when particles move almost along the magnetic field lines, the last equation will 'mimic' the effect of curvature energy loss.

We follow the particle trajectories during the phase of in-spiralling along the equatorial plane and subsequent propagation inside the vacuum gap. The particles are supposed to be initially at rest, with respect to the LNRF. Particles are initially injected in the equatorial plane (to mimic the injection from the thin accretion disc).

To study the electromagnetic emission from the accelerated particles we calculate, at each step of the integration of particle trajectory, the energy and power of synchrotron/curvature emission and ascribe this energy and power to a nominal 'photon' that is emitted along the direction of the particle motion. We subsequently trace the trajectory of each emitted photon from the emission point to infinity by integrating the equations of the geodesics of the Kerr metric.

Charged particles that reach the outer boundary of the gap, escape along the geodesics of the Kerr metric. The motion along the time-like geodesics of the Kerr metric is determined by the equations [50]

$$\begin{aligned}
r^2\dot{r} &= \sqrt{T^2 - \Delta(\mu^2 r^2 + (\Phi - aE)^2)},\\
r^2\dot{\phi} &= \Phi - aE + aT/\Delta,\\
r^2\dot{t} &= a\Phi - a^2E + (r^2+a^2)T/\Delta,
\end{aligned} \tag{22}$$

where E and Φ are the integrals of motion, which correspond to the conserved energy and angular momentum, μ is the particle mass and T is defined as $T = E(r^2+a^2) - \Phi a$. In the following, the cited energies of particles ejected from the gap are always the 'energies measured by an observer at infinity', i.e. the integrals of motion E, which enter the geodesic equations (22).

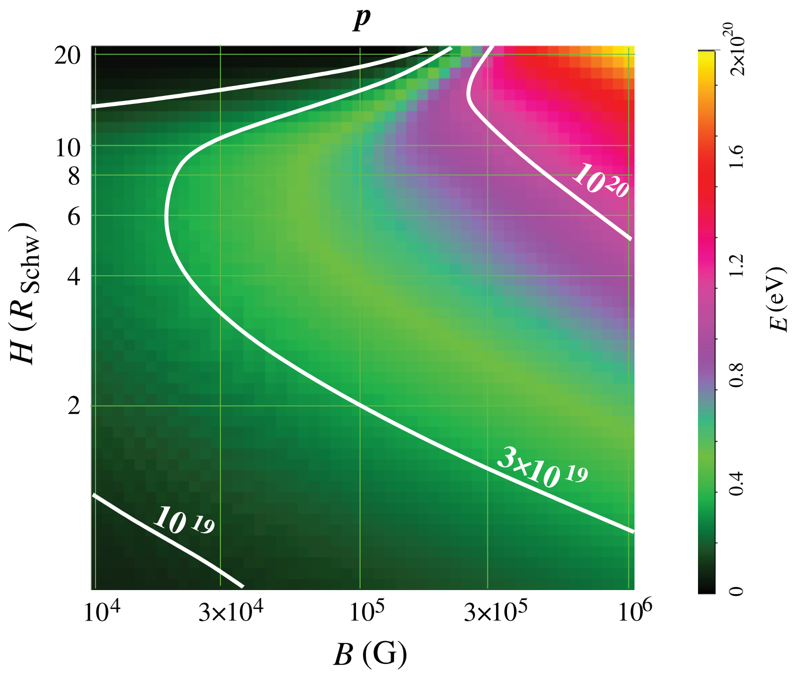

Figure 3. Energies of protons ejected from the vacuum gap (measured by an observer at infinity), as a function of the gap height H and the magnetic field B. The parameters are: BH mass $M = 3 \times 10^8 M_\odot$, rotation moment per unit mass $a = 0.99GM$ and the inclination angle of magnetic field $\chi = 5^\circ$. Protons are initially injected in the equatorial plane at a distance $R = 1.4r_\mathrm{H}$ from the BH.

4.2. Dependence of the maximal energy on the gap parameters

In this section, we study the dependence of the maximum energy to which protons can be accelerated on the geometry of the gap, such as on the basic parameters of the model: the gap height H, the inclination of magnetic field with respect to the BH rotation axis, χ, the BH mass M and on the magnetic field strength B.

Figure 3 shows the dependence of maximum energy of accelerated protons on the gap height H. We set the inclination angle of the magnetic field $\chi = 3^\circ$. One can see that for the assumed BH mass, $M_\mathrm{BH} = 3 \times 10^8 M_\odot$, the acceleration to energies above 10^{20} eV is possible only if the gap height is larger than $H > R_\mathrm{Schw}$, provided that the magnetic field near the horizon is extremely strong, $B > 3 \times 10^4$ G. One can notice that the increase of the gap height beyond a certain field-dependent limit does not lead to the further increase of the particle energies. This is explained by the decrease of the electric field strength (see equation (11)) and, as a consequence, the decrease of the acceleration rate far from the BH. Since the magnetic field is assumed to be asymptotically constant, the rate of the energy loss does not decrease with the distance, contrary to the acceleration rate. The combination of the decreasing acceleration rate and steady loss rate leads to the decrease of the particle energies at large distances. Obviously, the assumption of the asymptotically constant magnetic field, adopted in our toy model, does not hold in a realistic case, when the magnetic field is produced by the accreting matter.

Figure 4 shows the dependence of maximum energy on the inclination angle of magnetic field with respect to the rotation axis of the BH, χ. In our toy model, particles are initially

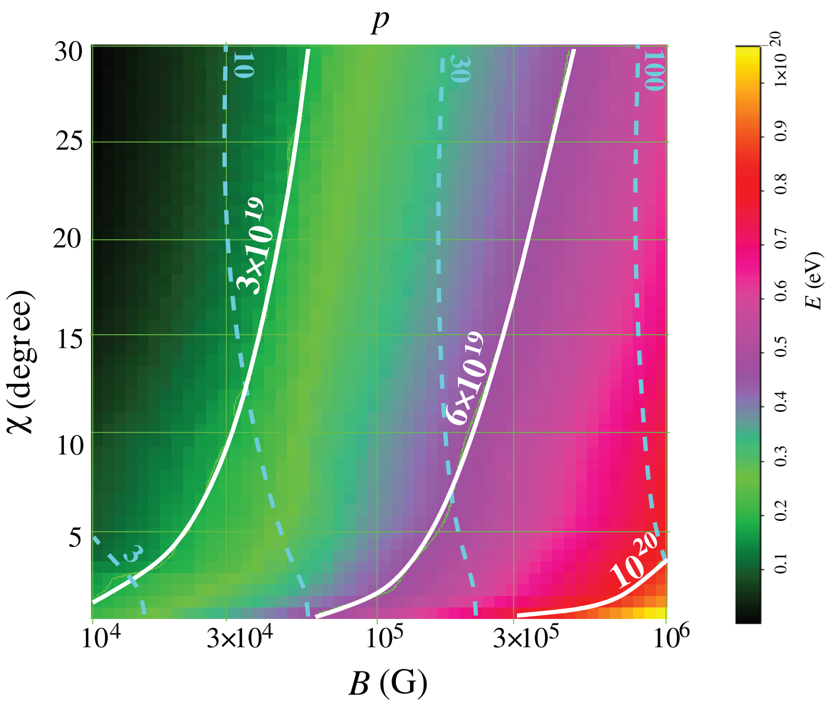

Figure 4. Energies of protons ejected from the vacuum gap (measured by an observer at infinity), as a function of the inclination angle of the magnetic field, χ and of the magnetic field strength B. The parameters of the calculation are: $M = 3 \times 10^8 M_\odot$, $a = 0.99GM$ and $H = 5R_{\rm Schw}$. Dashed cyan contours show the ratio of the electromagnetic to CR luminosity for the particular gap parameters.

supplied by the equatorial accretion disc, so that the initial positions of the particles are in the equatorial plane. One can see that the acceleration to energies above 10^{20} eV close to a BH of mass $5 \times 10^8 M_\odot$ is possible only if $\chi \ll 1$. The increase of the misalignment between the magnetic field and the BH rotation axis leads to the decrease of the maximal energies and to the increase of the power of electromagnetic emission that accompanies the acceleration process (cyan dashed curves in this figure are marked by the value of the ratio of the electromagnetic luminosity, $L_{\rm EM}$ to the UHECR luminosity, $L_{\rm UHECR}$).

The requirement on the alignment of the magnetic field can be somewhat relaxed in the case of higher BH mass or still higher magnetic field strength. In fact, since, in the 'energy loss saturated' regime the maximal energy grows as $B^{1/4}M^{1/2}$ (see equation (16)), the increase of the magnetic field by an order of magnitude results just in a slight correction of the maximal allowed misalignment angle, while an order of magnitude heavier BH accelerates particles to just a factor of three higher energies.

This is clear from figure 5 in which the dependence of the particle energies on the magnetic field and the BH mass is shown. From this figure one can see that at the energies $E \geqslant 10^{20}$ eV the relation (16) holds, so that at the levels $E = \text{const}$ one has $M \sim B^{-1/2}$. For a $10^9 M_\odot$ BH the energy 10^{20} eV is attainable already when the magnetic field is $B \sim 10^4$ G. However, the further increase of the magnetic field by two orders of magnitude, up to $B \sim 10^6$ G, results in an increase of the particle energies just by a factor of two.

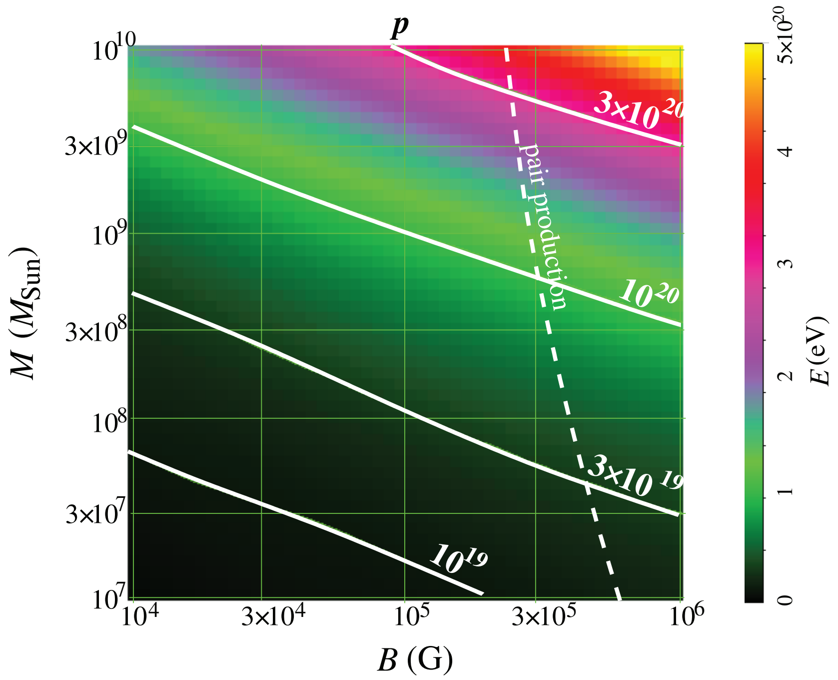

Figure 5. Maximal energy of protons ejected from the vacuum gap (measured by an observer at infinity), as a function of the BH mass M and magnetic field B. The parameters are: $a = 0.99GM$, $\chi = 5^\circ$ and $H = 5R_{\rm Schw}$. Particles are initially injected in the equatorial plane at a distance $R = 1.4r_{\rm H}$ from the BH.

5. Electromagnetic emission from the gap

5.1. Direct γ-ray emission from the particle acceleration in the gap

Protons accelerated near the BH horizon in the gap can produce γ-ray emission in the VHE band through several radiation mechanisms. For example, TeV emission can be synchrotron or curvature γ-ray emission which accompanies proton acceleration [25, 27]. The energy of curvature photons produced by protons accelerated to the energy $E_{\rm curv}$, given by equation (16), is

$$\epsilon_{\rm curv,p} \simeq 2\left[\frac{E_{\rm curv}}{10^{20}\,{\rm eV}}\right]^3\left[\frac{M}{3\times10^8 M_\odot}\right]^{-1}\left[\frac{\chi}{1^\circ}\right]{\rm TeV}. \tag{23}$$

Thus, the particle acceleration activity of the gap should reveal itself through the γ-ray emission in the VHE band. Figure 6 shows the numerically calculated dependence of the maximal energies of the γ-rays emitted by the gap on the physical parameters of the gap, M and B. One can see that for the range of parameters at which UHECR production is possible (i.e. above the thick white line with the mark '10^{20}' in this figure) the maximal energies of the γ-rays reach 1–100 TeV. Combining equations (16) and (23) one can find that $\epsilon_{\rm curv,p} \sim M^{1/2}B^{3/4}$ so that the lines $\epsilon_{\rm curv,p} = {\rm const}$ correspond to $M \sim B^{-3/2}$ in the figure.

The 'direct' γ-ray emission from the vacuum gap is highly anisotropic (in fact the opening angle of the emission cone is determined not only by the width of the gap, but also by the

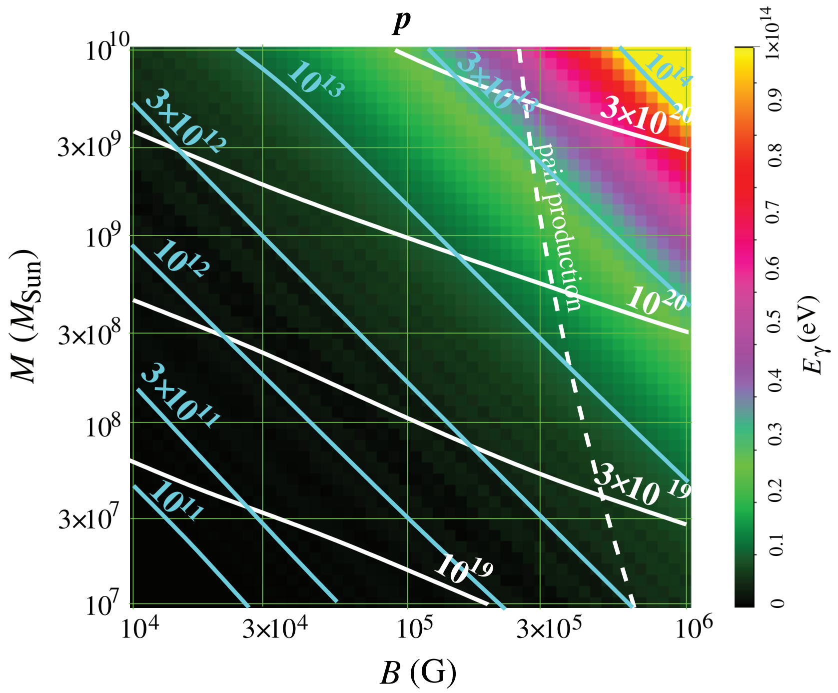

Figure 6. Colour and cyan contours: maximal energy of γ-ray quanta produced by the accelerated protons in the vacuum gap (measured in the LNRF), as a function of the BH mass and magnetic field. White contours show the maximal energies of the accelerated protons (see figure 5). Dashed line shows the values of M and B at which the pair production in the magnetic field sets on, on the distance scale of the inhomogeneity of the magnetic field. The parameters are: $a = 0.99GM$, $\chi = 5^\circ$ and $H = 5R_{\rm Schw}$. Protons are initially injected in the equatorial plane at a distance $R = 1.4r_{\rm H}$ from the BH.

deflections of the γ-ray trajectories by the BH gravitational field. Figure 7 shows the angular distribution of the average energies of the γ-rays emitted by particles accelerated in the gap. The highest energy photons are emitted in the direction of the magnetic field. The in-spiralling particles penetrate into the reconnection region mostly from the two opposite directions in the equatorial plane, in which the reconnection of the force-free surfaces starts at the largest distance (see the bottom panels of figure 2). This explains the appearance of the two emission regions at the opposite sides of the BH. The highest energy γ-rays are emitted in the directions of the southern and northern poles, along the direction of the magnetic field. Lower energy photons emitted closer to the equatorial plane are more strongly deviated and absorbed by the BH. A characteristic anisotropy of the γ-ray emission from the gap is preserved even if the magnetic field is not aligned with the BH rotation axis (see e.g. [22]).

In most of the sources, the magnetic field in the gap is not aligned with the line of sight toward the source, so that the direct γ-ray emission from the gap is not detectable. However, the 0.1–100 TeV γ-ray flux from the gap can be efficiently 'recycled' and 'isotropized' via the development of electromagnetic cascade in the infrared-to-ultraviolet photon background in the source (see e.g. [22]). This should lead to the redistribution of the primary γ-ray power over the lower energy photons, from radio to softer γ-rays.

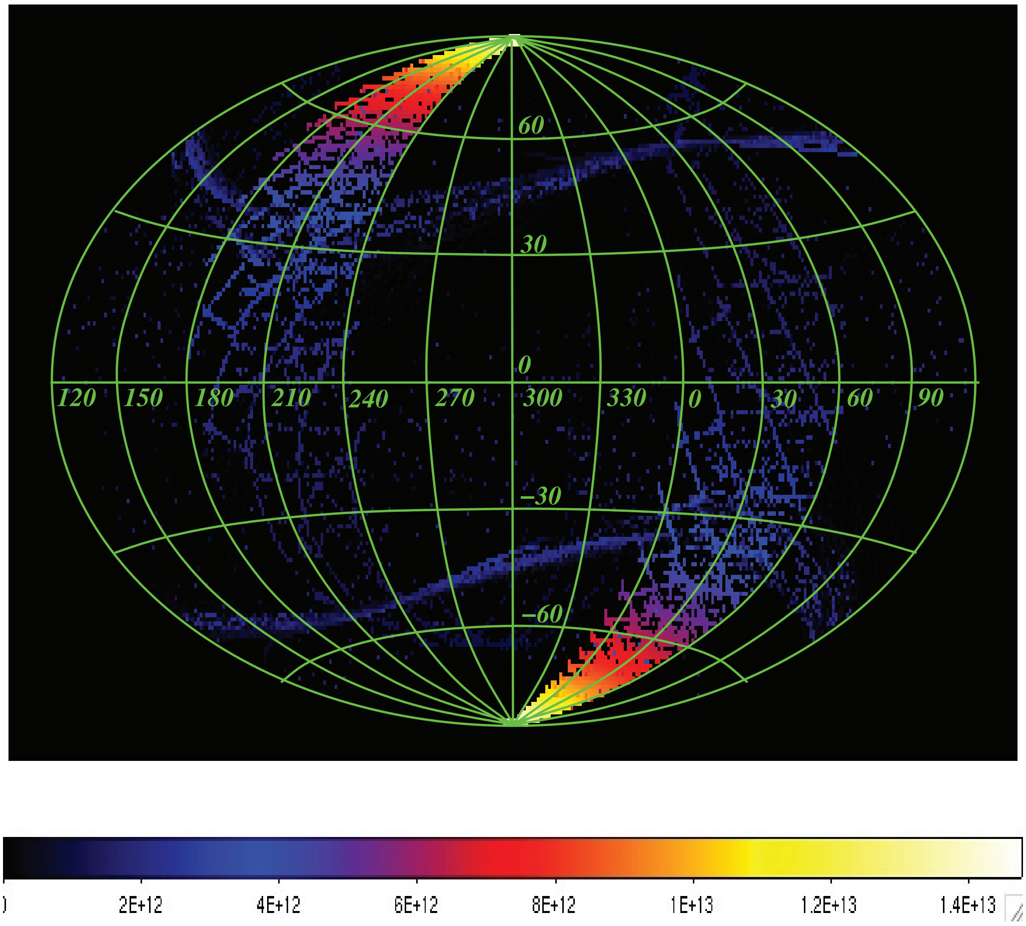

Figure 7. Anisotropy pattern of the γ-ray emission from the gap. The parameters are: $a = 0.99GM$, $\chi = 5^\circ$ and $H = 5R_{\mathrm{Schw}}$. Particles are initially injected in the equatorial plane at a distance $R = 1.4r_{\mathrm{H}}$ from the BH.

The details of the spectrum and anisotropy properties of the lower-energy electromagnetic emission from the cascades depend on the details of the soft photon and particle distributions, as well as on the (largely uncertain) structure of magnetic fields in the cascade regions. Calculation of these details has to take into account observational constraints on the matter, radiation and magnetic field properties in the source and in its surrounding medium (the accretion flow, the AGN jet, the interstellar medium of the source host galaxy, etc). Recent observations of the γ-ray emission from radio galaxies and blazars indicate that electromagnetic cascades initiated by the VHE γ-rays [24, 35] and/or by the accelerated protons [24, 59, 60] could play an important role in the physics of the AGN jets.

5.2. Power of direct γ-ray emission from the gap

The UHECR data [3] imply that the total flux of the CRs above the cutoff at $E \sim 10^{20}$ eV is about[6]

$$F(E > 10^{20}\mathrm{eV}) \simeq (0.3\text{–}1) \times 10^{-12}\,\mathrm{erg\,cm^{-2}\,s^{-1}}. \tag{24}$$

[6] This estimate is almost an order of magnitude lower than the one used in [27], which relied on the AGASA data that did not show a signature of cutoff.

If this flux is produced by $N_{\rm source} \sim 100$ UHECR sources at distances $D \sim 50$–$100\,{\rm kpc}$, the typical luminosity of an UHECR source is about

$$L_{\rm source} \simeq (10^{40}\text{–}10^{41}) \left[\frac{100}{N_{\rm source}}\right] {\rm erg\,s^{-1}}. \tag{25}$$

Such an estimate should be compared with an estimate of the power of the UHECR emission by a typical vacuum gap close to a supermassive BH in AGN, which can be obtained in the following way. At small inclination angles χ the area of the region of the reconnection of the force-free surfaces in the equatorial plane (see figure 2) is estimated as $\mathcal{A} \sim 2\pi r_{\rm H}^2 \sin\chi$. The maximal rate of injection of the charged particles into the gap through the reconnection region is

$$R_{\rm max} \simeq n_{\rm GJ}\mathcal{A}, \tag{26}$$

where $n_{\rm GJ}$ is filled with the GJ density, given by equation (1). The energy of each particle ejected from the gap is $E_{\rm curv}$, given by equation (16). This means that the maximal CR power of the gap is

$$L_{\rm CR,max} \simeq R_{\rm max} E_{\rm curv} \simeq 6\times 10^{42} A Z^{-5/4} \left[\frac{M}{10^8 M_\odot}\right]^{3/2} \left[\frac{B}{10^4\,{\rm G}}\right]^{5/4} \left[\frac{\chi}{1^\circ}\right]^{1/2} {\rm erg\,s^{-1}}, \tag{27}$$

where we have assumed $\theta \simeq \chi$. Comparing the estimates (25)–(27) one can see that the necessary CR power of the vacuum gaps near the supermassive BHs can be achieved already when the charged particles are injected into the gap at the rate $\sim(0.01$–$0.1)\,R_{\rm max}$.

If the sources of UHECR are supermassive BHs in the centers of galaxies, the acceleration to energies above $10^{20}\,{\rm eV}$ is possible only in the 'loss saturated' regime, in which the acceleration rate is balanced by the energy loss rate, for most of the trajectory of the particle. This means that the power of electromagnetic emission from the gap dominates over the power emitted in the form of the high-energy particles.

Even in the case of the almost aligned magnetic field, considered in this paper, the power of electromagnetic emission from a (several) $\times\, 10^8 M_\odot$ BH is at least a factor of 10–50 larger than the UHECR power, as soon as the energy 10^{20} eV is reached (see figure 8). From this figure, one can see that the lines $L_{\rm EM}/L_{\rm UHECR} = {\rm const}$ roughly correspond to $M \sim B^{-3/2}$. This behaviour is readily explained, if one takes into account that a simple estimate of $L_{\rm EM}/L_{\rm UHECR}$ can be obtained by comparing the total available potential difference in the gap, to its fraction spent on the particle acceleration (rather than on the electromagnetic emission)

$$\frac{L_{\rm EM}}{L_{\rm UHECR}} \simeq \frac{E_{\rm max}}{E_{\rm cur}} \simeq 1 Z^{5/4} A^{-1} \left[\frac{M}{10^8 M_\odot}\right]^{1/2} \left[\frac{B}{10^4\,{\rm G}}\right]^{3/4} \left[\frac{\chi}{1^\circ}\right]^{1/2}, \tag{28}$$

(the above equation is valid if $E_{\rm cur} < E_{\rm max}$).

If the magnetic field is aligned with the rotation axis, $\chi \ll 1$, the estimate of the electromagnetic power is much lower than the one found for a general case of misaligned magnetic field in [27]. This means that a typical electromagnetic luminosity of a nearby UHECR source is

$$L_{\rm EM},\ {\rm source} \geqslant (10\text{–}100) L_{\rm source} \sim (10^{41}\text{–}10^{43}) \left[\frac{100}{N_{\rm source}}\right] {\rm erg\,s^{-1}}. \tag{29}$$

Such a luminosity is at the level of the luminosities of the AGN in the local Universe.

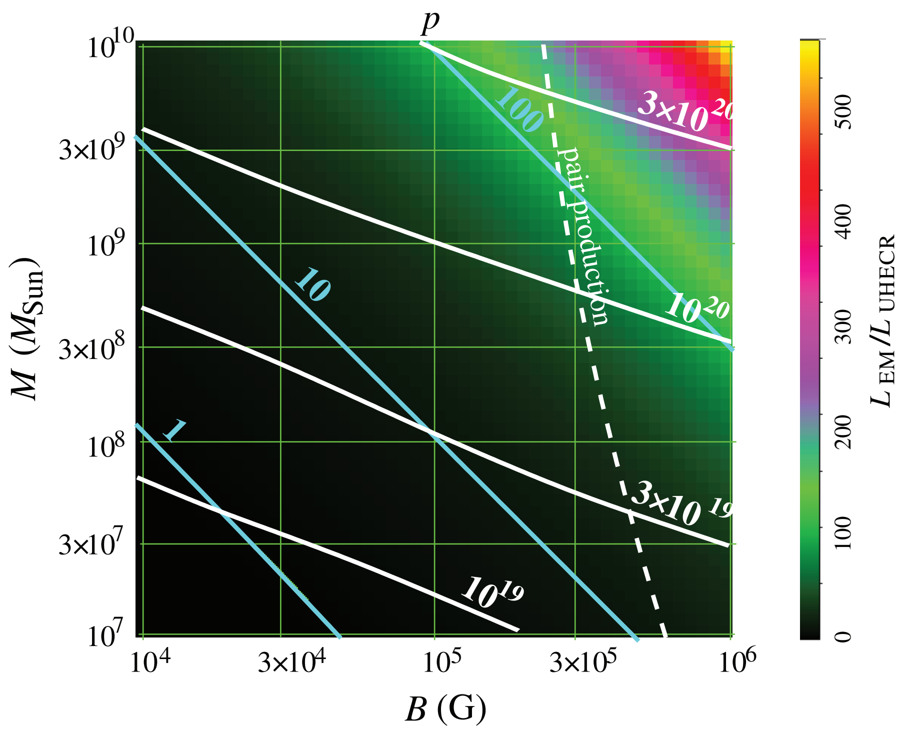

Figure 8. Ratio of the electromagnetic to the CR power of the gap, as a function of the BH mass M and magnetic field B. White contours show the maximal energies of the accelerated protons (see figure 5). The parameters are: $a = 0.99GM$, $\chi = 5^\circ$ and $H = 5R_{\rm Schw}$. Particles are initially injected in the equatorial plane at a distance $R = 1.4r_{\rm H}$ from the BH.

The primary power emitted in the form of the VHE γ-rays is, most probably, recycled via the cascading on the infrared backgrounds in the AGN central engine and in the host galaxy of the source. The cascading leads to the isotropization of the secondary emission, so that an observer is still able to detect a certain fraction of the primary power in the form of lower energy (e.g. synchrotron or inverse Compton) photons from the electromagnetic cascade.

5.3. Maximal height of the vacuum gap

The VHE γ-rays emitted by the accelerated particles can be absorbed in interactions with soft background photons or with magnetic fields. e^+e^- pairs produced in these interactions could initiate the development of an electromagnetic cascade in the gap which finally can 'short circuit' the vacuum gap and neutralize the parallel component of the electric field via charge redistribution. Similarly to the case of vacuum gaps in pulsar magnetospheres, the condition that the high-energy γ-ray quanta emitted from the gap do not produce e^+e^- pairs either in interaction with the strong magnetic field or with the soft background photons, can limit the height of the gap. Requiring that the gap height H is smaller than the mean free path of a γ-ray through the magnetic field, one finds [51]

$$H \leqslant D_{B\gamma} \approx 95 \left[\frac{10^4\,\mathrm{G}}{B_\perp}\right] \exp(8m_{\rm e}^3/3B_\perp\epsilon_{\rm curv})\,\mathrm{cm}. \tag{30}$$

In the case when the magnetic field is almost aligned with the BH rotation axis, the γ-rays are emitted along the direction of propagation of the accelerated particles, which, in turn, move along the magnetic field lines. For small inclination angles, the curvature radius of the magnetic field lines in the vacuum gap above the magnetic poles could be estimated as $R_B \sim R_{\rm Schw}/\sin(\chi)$. This means that the typical normal component of the magnetic field encountered by the γ-rays propagating inside the gap is

$$B_{\perp} \sim B \sin \chi, \tag{31}$$

so that for the case $\chi \sim 1^{\circ}$, considered here, the magnetic field component orthogonal to the particle and the γ-ray velocity is some two orders of magnitude weaker than the parallel one. This means that even if the magnetic field in the vacuum gap is very strong, $B \sim 10^6$ G, the typical mean free path of the γ-rays is larger than the characteristic distance scale of the problem (the Schwarzschild radius, $R_{\rm Schw}$). Thus, in the considered case of the gap with 'aligned' magnetic field, the pair production is not important over the entire range of BH masses studied in this paper. To check this conclusion we have included in the numerical code a calculation of the mean free path of the γ-rays emitted at each step of the particle trajectory and checked that condition (30) is never violated when the acceleration to energies above 10^{20} eV is possible in the range of parameters M, B, H and χ considered above.

Instead, in a realistic situation, the height of a vacuum gap with aligned magnetic field is most probably limited by the large-scale variations of the magnetic field, created by the accretion flow. Assuming that the magnetic field has a certain inhomogeneity scale R_B, one can find that the change of the field direction on this distance scale will lead to the loss of alignment between the trajectories of the γ-rays emitted by particles accelerated in the gap and the magnetic field, so that the normal component of the magnetic field becomes $B_{\perp} \sim B$. We have calculated the magnetic field strength at which the pair production on the distance scale R_B can set on, by substituting B instead of $B_{\perp}$ in the estimate of equation (30) in numerical calculations. As a result, we have found that the pair production can set on if the magnetic field strength is above the threshold shown by a white dashed line in figure 8. One can see that in the case when the magnetic field in the gap is aligned with the BH rotation axis, the pair production on the distance scale of inhomogeneity of the magnetic field can set on at the magnetic field strengths, $B \geqslant 10^5$ G.

Electromagnetic cascade that limits the height of the gap can be initiated by interactions of the γ-rays not only with the magnetic field, but also with soft infrared photons emitted by the accretion flow. In order to estimate the importance of this effect, one has to introduce additional assumptions about the radiative properties of the accretion flow. Curvature γ-rays with the energies $E_\gamma \sim 1$ TeV produce e^+e^- pairs mostly in interactions with the infrared photons of the energies $\epsilon \simeq 1[E_\gamma/1\,\mathrm{TeV}]^{-1}$ eV. Taking into account that the pair production cross-section peaks at the value $\sigma_{\gamma\gamma} \simeq 10^{-25}$ cm^2, one can find that the optical depth of the gap for the TeV γ-rays is

$$\tau_{\gamma\gamma} = \frac{L_{\rm IR}\sigma_{\gamma\gamma} H}{4\pi R_{\rm IR}^2 \epsilon} \simeq 0.2 \left[\frac{L_{\rm IR}|_{\epsilon=1(E_\gamma/1\,\mathrm{TeV})\,\mathrm{eV}}}{10^{42}\,\mathrm{erg\,s^{-1}}}\right]\left[\frac{R_{\rm IR}}{10^{16}\,\mathrm{cm}}\right]^{-2}\left[\frac{H}{10^{14}\,\mathrm{cm}}\right]\left[\frac{E_\gamma}{1\,\mathrm{TeV}}\right]. \tag{32}$$

Estimates of the optical depth of the gaps could be done if the constraints on the infrared luminosity of the AGN central engine and on the size of the infrared emission region are known from observations, on a source-by-source basis (see e.g. [22, 24]). For example, from the above estimate one can see that a gap of height $H \sim R_{\rm Schw} \sim 3 \times 10^{13}$ cm in the magnetosphere of a $M \sim 10^8 M_\odot$ BH surrounded by the accretion flow producing the infrared luminosity $L_{\rm IR} \sim 10^{42}\,{\rm erg\,s^{-1}}$ in a region of the size $R_{\rm IR} \sim 100 R_{\rm Schw}$ would not be closed as a result of the $\gamma\gamma$ pair production inside the gap, since $\tau_{\gamma\gamma} < 1$ in this case.

6. Acceleration of heavy nuclei

Up to now we have considered the acceleration of protons. However, our results can be generalized, in a straightforward way, to the case of acceleration of heavier nuclei, using the equations of section 3.2.

Heavy nuclei, like fully ionized iron, could be accelerated to higher energies, since their charge is $Z > 1$. However, nuclei with energies above 10^{20} eV are easily disintegrated in interactions with the infrared background photons which are present at the acceleration site, in the accelerator host galaxy, in the intergalactic space and in the Galaxy. The secondary nucleons produced in the photon disintegration have the energy $E_{\rm N} \simeq E/A$. Taking this into account, one can find that, if the nuclei are fully disintegrated, the assumption about the acceleration of nuclei does not result in an increase of the estimate of the maximal energies of protons reaching the detector on Earth. E.g. the critical energy (per nucleon), at which the transition to the loss-dominated regime of acceleration happens (see equation (18)),

$$E_{\rm crit,N} \simeq E_{\rm crit}/A \sim A^{1/3} Z^{-2/3} \tag{33}$$

scales as $A^{1/3}Z^{-2/3}$, a factor that is less than 1 for most of the primary nuclei. In the case of acceleration in the curvature loss-dominated regime, $E_{\rm cur,N} \simeq E_{\rm cur}/A \sim Z^{-1/4}$ does not depend on the atomic number A at all.

However, the assumption about full disintegration of the nuclei on the way from the source to the observer on Earth can not be valid in some particular cases. First, if the energies of the Fe nuclei are around 10^{20} eV, the mean free path of the nuclei through the extragalactic infrared photon background is ∼100 Mpc. This means that the nuclei accelerated near the supermassive BH in nearby galaxies can cover the entire distance from the host galaxy to the Milky Way without being photo disintegrated [52]. Next, if the heavy nuclei are accelerated close to the supermassive BH in the center of the Milky Way galaxy, they also can reach Earth without being photo disintegrated.

To verify if the heavy nuclei produced in a particular source (supermassive black holes in nearby AGN and normal galaxies) are likely to be photo disintegrated, one could notice that e.g. in the case of iron nuclei, the photo disintegration cross section, which peaks at a giant dipole resonance ($E_{\rm res} \sim 10$–30 MeV in the nucleus rest frame) is close to the $\gamma\gamma$ pair production cross section, $\sigma_{{\rm Fe}-\gamma} \simeq 60(A-Z)Z/A\,{\rm mbar\,MeV}/E_{\rm res} \lesssim 10^{-25}\,{\rm cm}^2$ [61, 62]. This means that the condition that the optical depth of the source with respect to the photo disintegration is less than one imposes a constraint on the luminosity and/or size of the source, similar to the constraint following from the condition $\tau_{\gamma\gamma} < 1$ (see equation (32)). Iron nuclei of energy $E_{\rm Fe} \sim 10^{20}$ eV interact most efficiently with far-infrared photons of energies $\epsilon_{\rm FIR} \simeq 3 \times 10^{-2}[E_{\rm Fe}/10^{20}\,{\rm eV}]^{-1}$ eV, so that the restriction on the optical depth with respect to the photo disintegration imposes a constraint on the size and luminosity of the source and of its host galaxy in the far-infrared energy band.

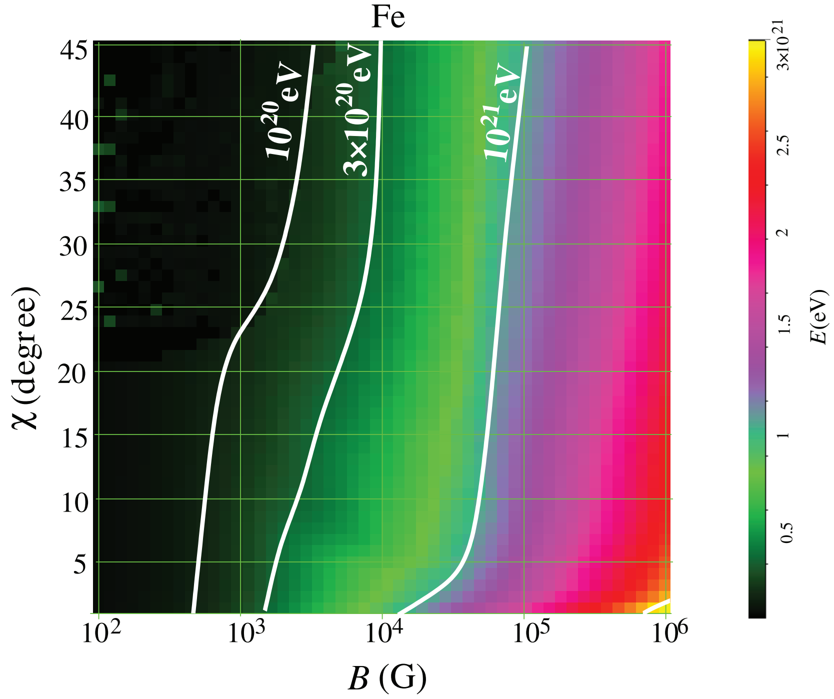

Figure 9. Same as in figure 4 but for the case of acceleration of iron nuclei.

The case of the acceleration of heavy nuclei differs from the case of proton acceleration in two important aspects: the higher mass of the nucleus (and, respectively, lower Lorentz factor) results in the reduction of the rate of the curvature energy loss and of the energies of the quanta of curvature radiation. Because of the lower energies of the curvature radiation quanta, pair production, which could limit the size of the gap (see previous section), sets on at higher values of the magnetic field. In addition, the electromagnetic luminosity of a source accelerating nuclei to energies $\sim 10^{20}$ eV could be lower than that of the source accelerating protons to $\sim 10^{20}$ eV.

Figures 9 and 10 show the numerically calculated maximal energies of accelerated particles and ratio of the electromagnetic to UHECR luminosity, as a function of M, B and χ, in the case of acceleration of Fe nuclei. The region of parameter space in which the acceleration proceeds in the 'loss-free' regime (i.e. the estimate of the maximal energy is given by equation (14)) is the black triangle in the lower left corner of figure 10. One can see that in spite of the moderate BH masses (down to $M \sim 10^7 M_\odot$) and/or moderate magnetic fields (down to $B \sim 10^3$ G in the case of a $10^9 M_\odot$ BH), acceleration up to energies $> 10^{20}$ eV is possible in this regime.

As an example, let us consider the particularly interesting case of particle acceleration near the supermassive BH in the center of the Milky Way galaxy, which hosts a BH of mass $M \sim 3 \times 10^6 M_\odot$ [53] (horizontal red line in figure 10). From figure 10 one can see that such a BH can accelerate iron nuclei up to energies $\sim 10^{19}$ eV if the magnetic field around it reaches $B \sim 5 \times 10^3$ G. The energy loss in this case is much smaller than the power of the CR emission $L_{\mathrm{EM}}/L_{\mathrm{UHECR}} = 5 \times 10^{-4}$. Fe nuclei with energies 10^{18-19} eV produced in the Galaxy are assumed to dominate the CR flux in this energy band in certain models explaining the 'ankle' feature of the CR spectrum [54]. In order to explain the observed CR flux at 10^{18} eV $F(10^{18}\,\mathrm{eV}) \simeq 200$ eV (cm^{-2} s^{-1} sr^{-1}) [3], the CR luminosity of a source in the Galactic

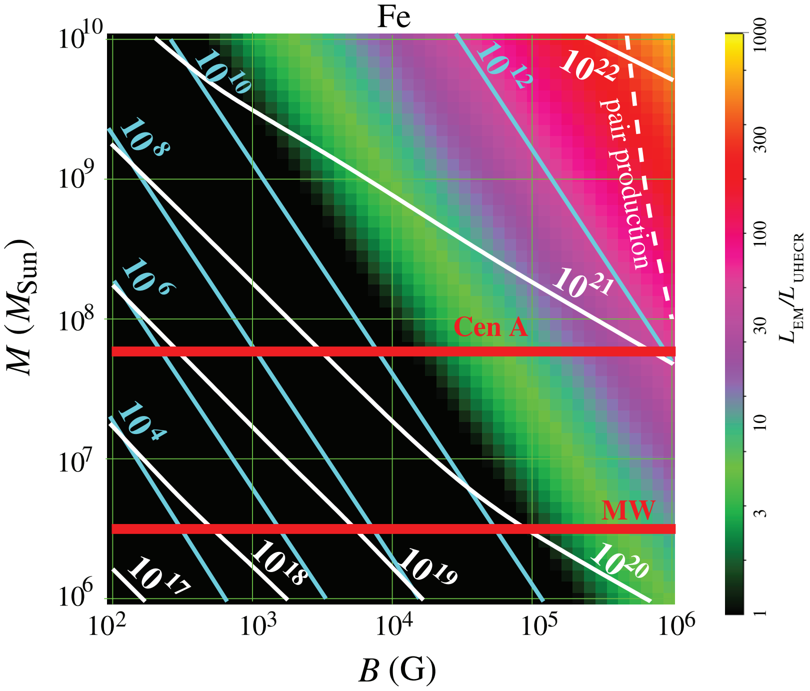

Figure 10. Same as in figure 8 but for the case of acceleration of iron nuclei. The masses of the BH in the center of the Milky Way and in the nucleus of Cen A are marked by red horizontal lines. The white contours show the maximal energies of the accelerated Fe nuclei (in eV). Cyan contours show the maximal energies of the γ-rays emitted by the nuclei (in eV). The white dashed line shows the limit at which pair production on the distance scale of inhomogeneity of the magnetic field sets on.

Center should be $L_{Fe} \sim 3 \times 10^{36}\,\mathrm{erg\,s^{-1}}$ (the luminosity can be still lower if the Fe nuclei diffuse through the Galactic magnetic field). From figure 10 one can see that the power of electromagnetic emission, which accompanies iron nuclei acceleration, could be as low as $L_{EM} \leqslant 10^{-3} L_{Fe}$, which is much less than the observed luminosity of the Galactic Center in the TeV band ($\sim 10^{35}\,\mathrm{erg\,s^{-1}}$ [55]). Of course, relaxing the assumption of approximate alignment of magnetic field with the BH rotation axis would result in a higher estimate of the electromagnetic luminosity. However, as is clear from equation (28), even in the loss-saturated regime of particle propagation in the gap, the power of electromagnetic emission increases by a factor of $\sim$10 as the inclination angle of the magnetic field increases from several degrees to $\chi \sim 1$. Thus, even in the absence of alignment of the magnetic field, the electromagnetic emission that would accompany acceleration of the iron nuclei to energies $\sim 10^{18-19}$ eV close to the Galactic Center BH would not be accompanied by significant electromagnetic emission.

7. Discussion and conclusions

In this paper, we have considered proton and heavy nuclei acceleration in the vicinity of the horizon of supermassive BHs. We have shown that proton acceleration by a large-scale electric field induced by the rotation of the BH can result in the production of CRs with energies above

10^{20} eV, provided that the magnetic field in the acceleration region is almost aligned with the BH rotation axis (to better than a few degrees, for a reasonable range of BH masses and magnetic field strengths $10^8 M_\odot \leqslant M_{\rm BH} \leqslant 10^{10} M_\odot$ and $10^4\,{\rm G} \leqslant B \leqslant 10^6\,{\rm G}$).

We have found that in the particular case of a rotating BH accreting through an equatorial disc, vacuum gaps, in which the large-scale electric field is not neutralized by redistribution of charges, form above the polar cap regions of the BH (see figure 1). In the case of a magnetic field exactly aligned with the BH rotation axis, charged particles from the equatorial accretion flow cannot penetrate into the polar cap regions (and, therefore, cannot be accelerated). However, as soon as the magnetic field is misaligned with the BH rotation axis, the charged particles that are initially injected at large distances into the equatorial plane, drift along the equatorial plane toward the BH, until they reach the region of 'reconnection' of the force-free surfaces close to the BH horizon (figure 2). As soon as the particles from the equatorial plane penetrate into the reconnection region, they 'leak' into the vacuum gaps above the polar caps and are ejected to infinity with high energies. Numerical modelling of particle transport and acceleration close to the BH has enabled us to calculate the dependence of the maximal attainable energies of the accelerated particles, as well as of the properties of electromagnetic emission produced by the accelerated particles, on the physical parameters, such as the BH mass M, the magnetic field B, the inclination of the magnetic field χ and the gap height H (see figures 3–6 and 8).

We have found that if the magnetic field is aligned to within several degrees with the rotation axis, the electromagnetic luminosity of the gap is just 10–50 times larger as compared to its UHECR ($E > 10^{20}$ eV) proton luminosity. A simple estimate has led us to the conclusion that the resulting electromagnetic luminosity of the gap is of the order of the bolometric luminosity of a typical AGN in the local Universe, which makes the central engines of the AGN plausible candidates for astrophysical UHECR sources.

In the case of acceleration of heavy nuclei, acceleration to energy $\geqslant 10^{20}$ eV is possible for a much wider range of BH masses and magnetic fields, without strong requirement on alignment (see figure 9). In particular, even a BH of mass $\sim 3 \times 10^6 M_\odot$ (like the one in the center of the Milky Way galaxy [56]) can accelerate iron nuclei to energies above 10^{18} eV when the magnetic field is several hundred Gauss, in the regime when the power of electromagnetic emission from the accelerator is negligible, compared to its CR power. Similarly, the nearest AGN Centaurus A, that hosts a BH with mass $\sim 6 \times 10^7 M_\odot$ [57], can produce Fe nuclei with energies of 10^{20} eV if the magnetic field close to the BH horizon is above 3×10^3 G (see figure 10). It is important to understand how often the strong alignment between the magnetic field and the BH spin, $\zeta <$ (several)$^\circ$, arises in AGN. This will help to discriminate between protons and heavy nuclei at the highest energies, $E \geqslant 10^{20}$ eV.

The energy spectra of CRs produced by individual sources via the considered particle acceleration mechanism are sharply peaked at nearly maximum energy, similar to the spectra of high-energy particles produced in linear accelerators. This feature could potentially distinguish the presented mechanism from the conventional shock acceleration mechanism, which typically gives power-law spectra $\mathrm{d}N/\mathrm{d}E \sim E^{-\alpha}$ with $\alpha \geqslant 2$. The typical intrinsic spectra of the UHECR sources can be found with higher statistics of UHECR events, $N > 100$ events at $E > 60$ EeV [58].

References

[1] Greisen K 1966 End to the cosmic ray spectrum? *Phys. Rev. Lett.* **16** 748
[2] Zatsepin G T and Kuzmin V A 1966 *Pisma Zh. Eksp. Teor. Fiz.* **4** 114
Zatsepin G T and Kuzmin V A 1966 Upper limit of the spectrum of cosmic rays *JETP Lett.* **4** 78 (Engl. Transl.)
[3] Abbasi R *et al* (HiRes Collaboration) 2007 arXiv:astro-ph/0703099
[4] Roth M (PAO Collaboration) 2007 Measurement of the UHECR energy spectrum using data from the surface detector of the Pierre Auger Observatory arXiv:0706.2096 [astro-ph] online at http://www.auger.org/technical_info/spectrum2007/spectrum_icrc07.html
[5] Abraham J *et al* (Pierre Auger Collaboration) 2007 *Science* **318** 938
[6] Abraham J (PAO Collaboration) 2008 *Astropart. Phys.* **29** 188
[7] Gorbunov D, Tinyakov P, Tkachev I and Troitsky S V 2008 *JETP Lett.* **87** 461
[8] Wibig T and Wolfendale A W 2007 arXiv:0712.3403
[9] Fargion D 2008 arXiv:0801.0227
[10] Gorbunov D S, Tinyakov P G, Tkachev I I and Troitsky S V 2008 arXiv:0804.1088
[11] Abassi R U *et al* 2008 arXiv:0804.0382
[12] Moskalenko I V, Stawarz L, Porter T A and Cheung C C 2008 arXiv:0805.1260
[13] Ptitsyna K and Troitsky S 2008 arXiv:0808.0367
[14] Gureev S and Troitsky S 2008 arXiv:0808.0481
[15] Berezinsky V S and Grigor'eva S I 1977 *Proc. 15th Int. Cosmic Ray Conf. (Plovdiv, Bulgaria)*
Berezinsky V S, Bulanov S V, Dogiel V A, Ginzburg V L and Ptuskin V S 1990 *Astrophysics of Cosmic Rays* (Amsterdam: Elsevier)
[16] Fraschetti F and Melia F 2008 arXiv:0809.3686
[17] Berezhko E G 2008 *Adv. Space Res.* **41** 429
[18] Atoyan A and Dermer C D 2008 arXiv:0808.0161
[19] Aharonian F A *et al* 2006 *Science* **314** 1424
[20] Albert J *et al* 2007 *Astrophys. J.* **669** 862
[21] Aharonian F *et al* 2007 *Astrophys. J.* **664** L71
[22] Neronov A and Aharonian F 2007 *Astrophys. J.* **671** 85
[23] Krawczynski H 2007 *Astrophys. J.* **659** 1063
[24] Neronov A, Semikoz D and Sibiryakov S 2008 *Mon. Not. R. Astron. Soc.* **391** 949
[25] Levinson A 2000 *Phys. Rev. Lett.* **85** 912
[26] Aharonian F A, Belyanin A A, Derishev E V, Kocharovsky V V and Kocharovsky V V 2002 *Phys. Rev.* D **66** 023005 (arXiv:astro-ph/0202229)
[27] Neronov A, Tinyakov P and Tkachev I 2005 *Zh. Eksp. Teor. Fiz.* **100** 744
Neronov A, Tinyakov P and Tkachev I 2005 *J. Exp. Theor. Phys.* **100** 656 (Engl. Transl.)
[28] Lyne A and Graham-Smith F 2005 *Pulsar Astronomy* (Cambridge: Cambridge University Press)
[29] Wald R M 1974 *Phys. Rev.* D **10** 1680
[30] Bicak J and Dvorak L 1976 *Gen. Rel. Gravit.* **7** 959
Bicak J and Janis V 1985 *Mon. Not. R. Astron. Soc.* **212** 899
[31] Lovelace R V E 1976 *Nature* **262** 649
[32] Lovelace R V E, MacAuslan J and Burns M L 1979 *AIP Conf. Proc.* **56** 399
[33] Blandford R D and Znajek R L 1977 *Mon. Not. R. Astron. Soc.* **179** 433
[34] Beskin V S, Istomin Ya N and Par'ev V I 1992 *Sov. Astron.* **36** 642
[35] Neronov A, Semikoz D, Aharonian F and Kalashev O 2002 *Phys. Rev. Lett.* **89** 051101
[36] Neronov A Y and Semikoz D V 2003 *New Astron. Rev.* **47** 693
[37] Neronov A Y and Semikoz D V 2002 *Phys. Rev.* D **66** 123003
[38] Boldt E and Ghosh P 1991 *Mon. Not. R. Astron. Soc.* **307** 491

[39] Bardeen J M and Petterson J A 1975 *Astrophys. J.* **195** L65
[40] Shakura N I and Syunyaev R A 1973 *Astron. Astrophys.* **24** 337
[41] Narayan R and Yi I 1994 *Astrophys. J.* **428** L13
[42] Rees M J, Begelman M C, Blandford R D and Phinney E S 1982 *Nature* **295** 17
[43] Goldreich P and Julian W H 1969 *Astrophys. J.* **157** 869
[44] Blandford R D and Payne D G 1982 *Mon. Not. R. Astron. Soc.* **199** 883
[45] Komissarov S 2005 *Mon. Not. R. Astron. Soc.* **359** 801
[46] Bardeen J M, Press W H and Teukolsky S A 1972 *Astrophys. J.* **178** 347
[47] Thorne K S, Price R H and Macdonald D A 1986 *Black Holes: The Membrane Paradigm* (New Haven, CT: Yale University Press)
[48] Press W H *et al* 1992 *Numerical Recipes in C: The Art of Scientific Computing* (Cambridge: Cambridge University Press) online at http://www.nr.com/
[49] Landau L D and Lifshitz E M 1980 *The Classical Theory of Fields* (Amsterdam: Elsevier)
[50] Carter B 1968 *Phys. Rev.* **174** 1559
[51] Erber T 1966 *Rev. Mod. Phys.* **38** 626
[52] Allard D *et al* 2006 *J. Cosmol. Astropart. Phys.* JCAP09(2006)005
[53] Genzel R *et al* 2000 *Mon. Not. R. Astron. Soc.* **317** 348
[54] Bird D J *et al* 1994 *Astrophys. J.* **424** 491
[55] Aharonian F *et al* 2004 *Astron. Astrophys.* **425** L13
[56] Schodel R *et al* 2002 *Nature* **419** 694
[57] Haring-Neumayer N, Cappellari M, Rix H W, Hartung M, Prieto M A, Meisenheimer K and Lenzen R 2006 *Astrophys. J.* **643** 226
[58] Kachelriess M, Parizot E and Semikoz D V 2007 arXiv:0711.3635
[59] Mannheim K 1993 *Astron. Astrophys.* **269** 67
[60] Bottcher M, Reimer A and Marscher A P 2008 arXiv:0810.4864
[61] Stecker F W and Salamon M H 1999 *Astrophys. J.* **512** 521
[62] Khan E *et al* 2005 *Astropart. Phys.* **23** 191